Lecture Notes in Electrical Engineering 1100

Xuzhu Dong
Li Cai *Editors*

The Proceedings of 2023 4th International Symposium on Insulation and Discharge Computation for Power Equipment (IDCOMPU2023)

Volume I

Springer

Lecture Notes in Electrical Engineering

Volume 1100

The book series *Lecture Notes in Electrical Engineering* (LNEE) publishes the latest developments in Electrical Engineering—quickly, informally and in high quality. While original research reported in proceedings and monographs has traditionally formed the core of LNEE, we also encourage authors to submit books devoted to supporting student education and professional training in the various fields and applications areas of electrical engineering. The series cover classical and emerging topics concerning:

- Communication Engineering, Information Theory and Networks
- Electronics Engineering and Microelectronics
- Signal, Image and Speech Processing
- Wireless and Mobile Communication
- Circuits and Systems
- Energy Systems, Power Electronics and Electrical Machines
- Electro-optical Engineering
- Instrumentation Engineering
- Avionics Engineering
- Control Systems
- Internet-of-Things and Cybersecurity
- Biomedical Devices, MEMS and NEMS

For general information about this book series, comments or suggestions, please contact leontina.dicecco@springer.com.

To submit a proposal or request further information, please contact the Publishing Editor in your country:

China

Jasmine Dou, Editor (jasmine.dou@springer.com)

India, Japan, Rest of Asia

Swati Meherishi, Editorial Director (Swati.Meherishi@springer.com)

Southeast Asia, Australia, New Zealand

Ramesh Nath Premnath, Editor (ramesh.premnath@springernature.com)

USA, Canada

Michael Luby, Senior Editor (michael.luby@springer.com)

All other Countries

Leontina Di Cecco, Senior Editor (leontina.dicecco@springer.com)

**** This series is indexed by EI Compendex and Scopus databases. ****

Xuzhu Dong · Li Cai
Editors

The Proceedings of 2023 4th International Symposium on Insulation and Discharge Computation for Power Equipment (IDCOMPU2023)

Volume I

Springer

Editors
Xuzhu Dong
School of Electrical Engineering
and Automation
Wuhan University
Wuhan, China

Li Cai
School of Electrical Engineering
and Automation
Wuhan University
Wuhan, China

ISSN 1876-1100 ISSN 1876-1119 (electronic)
Lecture Notes in Electrical Engineering
ISBN 978-981-99-7392-7 ISBN 978-981-99-7393-4 (eBook)
https://doi.org/10.1007/978-981-99-7393-4

This Springer imprint is published by the registered company Springer Nature Singapore Pte Ltd.
The registered company address is: 152 Beach Road, #21-01/04 Gateway East, Singapore 189721, Singapore

Paper in this product is recyclable.

Contents

The Effect of Contact Structure on Electromagnetic Force

Min Li, Baochun Song, and Anthony Papillon

Abstract In order to improve the performance of vacuum interrupter, two types of radial magnetic field (RMF) contact structure were designed for electromagnetic force research. Electromagnetic force of arc and electric repulsion of move contact was simulated analysis by Ansys software at 25 kA. The electric repulsion of move contact can be decreased to 4% by improving contact structure at short time withstand current. It can improve the performance of short time withstand current (STC), peak withstand current and earthing switch making. The electromagnetic force direction of arc can be improved by improving contact structure. It can avoid arc erosion in a small area of contact and increase electric endurance performance. The electromagnetic force of arc can be increased by contact 15° dislocation assemble. It can increase the electric endurance performance of contact. The electric repulsion of move contact is about 190 N at 0.5 mm contact gap with arc for both contact structures.

Keywords Vacuum interrupter · Simulation · Electromagnetic force

1 Introduction

Vacuum circuit breaker (VCB) has been widely used in middle voltage electric network [1, 2]. Vacuum interrupter (VI) is the core part of VCB [3], which is used for current conduct, fault current breaking and shot time withstand. In order to reach these requirements, the VI contact need design to different shapes. But they can be classified to axial magnetic field (AMF) or RMF. Most of researchers focus on breaking performance of contact. Different contact structures have been designed and tested. The vacuum arc of RMF will rotate fast on the contact surface to avoid arc erosion in the small area [4]. In order to decrease the arc erosion of RMF, arc

M. Li (✉) · B. Song
Schneider Electric (Xiamen) Switchgear Equipment Co., Ltd, Xiamen 361000, China
e-mail: lim2013pg@126.com

A. Papillon
Schneider Electric Co., Ltd, Grenoble, France

X. Dong and L. Cai (eds.), *The Proceedings of 2023 4th International Symposium on Insulation and Discharge Computation for Power Equipment (IDCOMPU2023)*, Lecture Notes in Electrical Engineering 1100, https://doi.org/10.1007/978-981-99-7393-4_1

rotate speed need increase by increasing electromagnetic force of arc [5]. In order to pass shot time withstand current (STC) test for a period of time (1–4 s), the VCB must be able to open the contact after STC. Thus, the contact welding force must be minimized. The AMF VI has an additional attractive force due to the parallel current flowing in the fixed and moved AMF coils behind the contacts [6]. So, AMF is benefit for STC test. But RMF VI has a repulsive blow-off force due to the reverse current flowing in two electrodes.

In order to improve the performance of VI, some researchers combine AMF and RMF [7]. Many commercial simulation software was used for simulation, like Ansys [8], COMSOL [9] and et al. This paper researched the Electromagnetic force of arc and electric repulsion of move contact by Ansys software at 25 kA to improve the STC and breaking performance.

2 Contact Structures and Simulation Method

The contact structures are shown in Fig. 1. Two contact structures were designed. The diameter of contact is 44 mm. the thickness of contact is 8 mm. V1 is a simple, flat spiral contact. V2 is an improved spiral contact which has slope, contact surface and counterbore structure.

The electric repulsion simulation models of moved contact are shown in Fig. 2. A column was used to simulate the real contact area, its diameter is 1 mm and the height is 0.5 mm. its color is gray in the model. There are two real contact areas were designed in V1, one is near central hole, one is in the same position with that in V2. Because V2 has 4 contact area, 4 columns were designed in V2 model. The assemble method of moved contact and fixed contact is fully aligning.

The electromagnetic force simulation models of arc are shown in Fig. 3. The arc model was designed as a column, its diameter is 1 mm and height is 0.5 mm. The arc model color is gray. There are two arc model positions in V1 and one arc model position in V2.

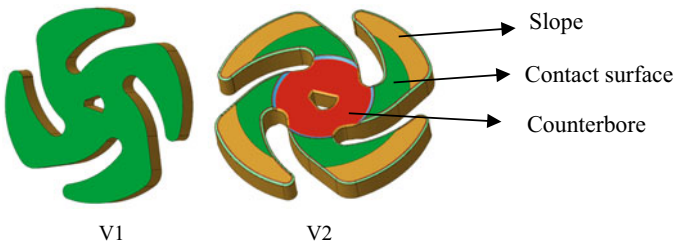

Fig. 1 Contact structures

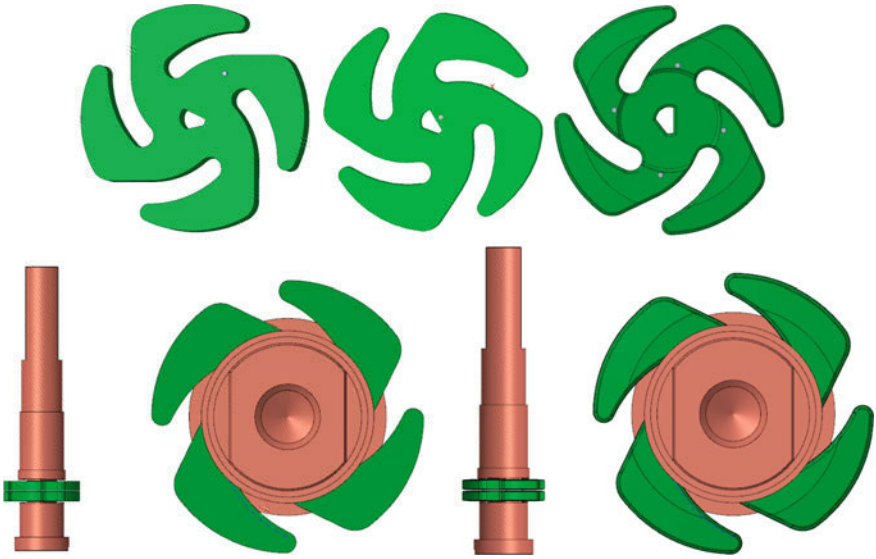

Fig. 2 Electric repulsion simulation models of moved contact

Fig. 3 Electromagnetic force simulation models of arc

In order to research the contact assemble effect on electromagnetic force of arc, two contact assemble models were designed as shown in Fig. 4. One is fully aligning assemble of fixed contact and moved contact, one is 15° dislocation assemble.

3 Simulation Results

The electric repulsion force of moved contact at closing with 25 kA STC is shown in Table 1. It shows that the electric repulsion force of V1 is about 23 times than that of V2. V2 is much benefit for STC to decrease contact welding. The contact area of V1 and the assemble method of V2 have some effect of electric repulsion force of moved contact, but it is little.

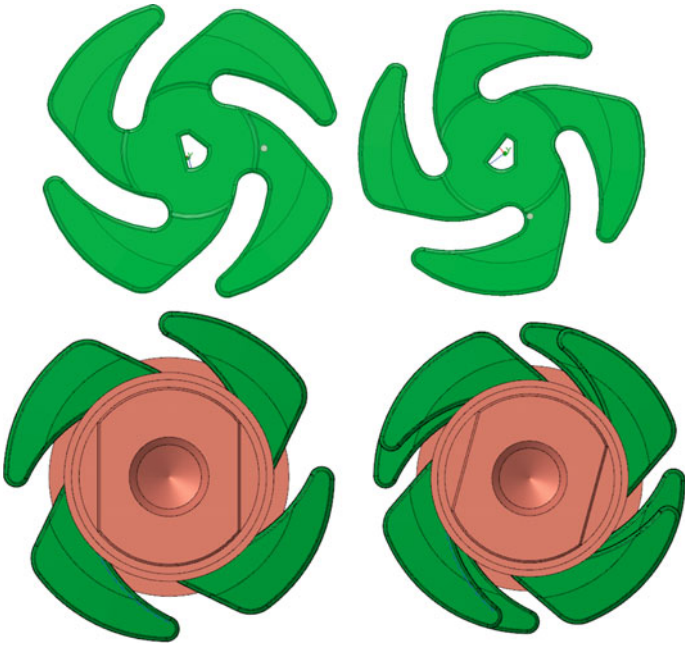

Fig. 4 Two contact assemble models

Table 1 Electric repulsion force of moved contact at closing with 25 kA STC (N)

Contact structure	Electric repulsion force
V1 with contact area like V2	192.7
V1 with contact area near central hole	182.5
V2 with fully aligning contact assemble	8.1
V2 with 15° dislocation assemble	7.3

The electric repulsion force of moved contact at 0.5 mm contact gap with 25 kA current is shown in Table 2. It shows that the electric repulsion force of V1 is similar than that of V2. The electric repulsion force of V2 with 15° dislocation assemble is 4.3 N higher than that with fully aligning contact assemble. Electric repulsion force of moved contact of RMF VI at small contact gap can help to increase open speed, so, it is benefit for VI breaking.

Magnetic strength of V2 at closing with 25 kA STC is shown in Fig. 5. The maximum value is 2.7 T which is around the column surface. There have radial and tangential magnetic field.

Magnetic strength of moved contact at 0.5 mm contact gap is shown in Fig. 6. The maximum value is little different from 10.5 to 11.4 T. The maximum value happened around the arc column surface. But the maximum value direction is different. Most of magnetic field is tangential.

Table 2 Electric repulsion force of moved contact at 0.5 mm contact gap with 25 kA current (N)

Contact structure	Electric repulsion force
V1 with contact area like V2	192.7
V1 with contact area near central hole	182.5
V2 with fully aligning contact assemble	191.7
V2 with 15° dislocation assemble	196.0

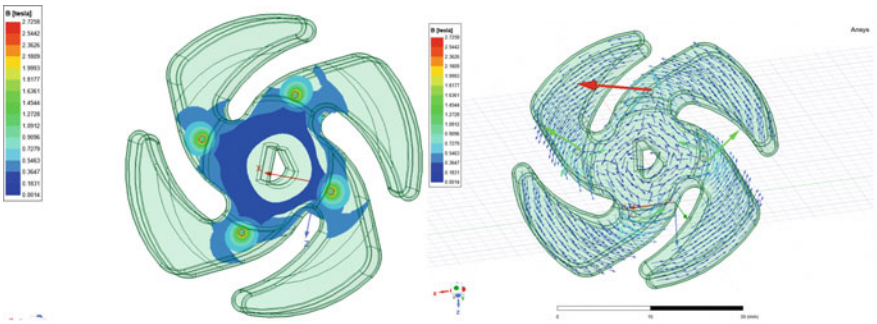

Fig. 5 Magnetic strength of V2 at closing with 25 kA STC

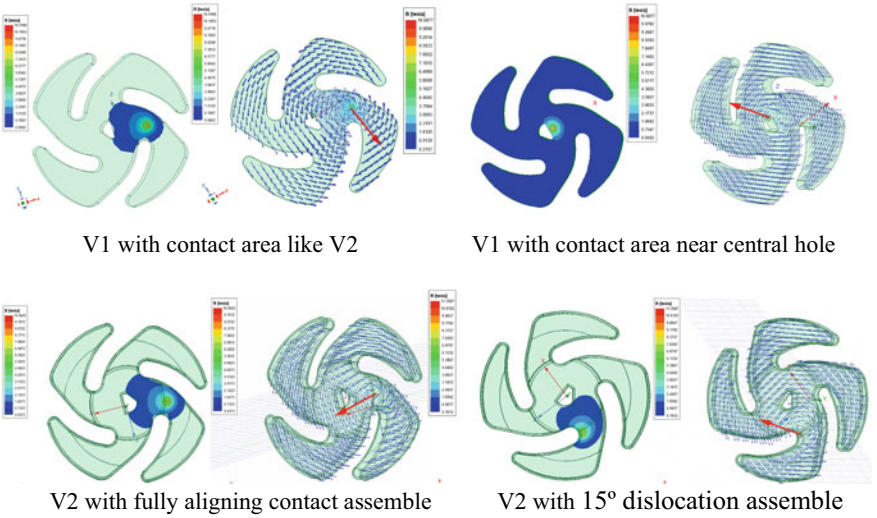

Fig. 6 Magnetic strength of moved contact at 0.5 mm contact gap

Volume force density of arc at 0.5 mm contact gap is shown in Fig. 7. The electromagnetic force of arc at 0.5 mm contact gap is shown in Table 3. It shows that the maximum electromagnetic force of arc is 13.1 N at V1 with contact area near central hole, but the force direction is −x. This force will push the arc go to the center of contact, which will make a high erosion at contact center area. The force direction of V1 with contact area like V2 is x, which will push the arc go to the contact edge and erosion the edge. The force direction of V2 is −x and z, it will push arc rotate around the petal. The force value of V2 with 15° dislocation assemble is higher than that of V2 with fully aligning contact assemble. It can decrease the arc erosion on contact.

Magnetic strength of arc at 0.5 mm contact gap is shown in Fig. 8. The maximum value of magnetic strength of arc is from 10.7 to 11.4 T at different situation, it is not much different. But the magnetic strength distribution is different.

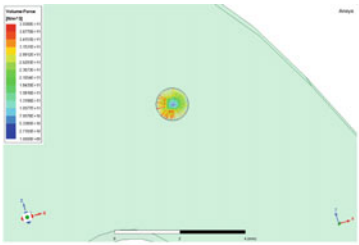

V1 with contact area like V2

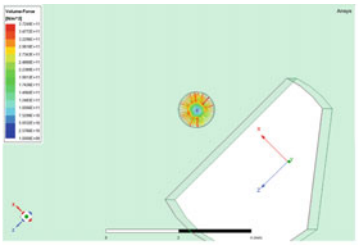

V1 with contact area near central hole

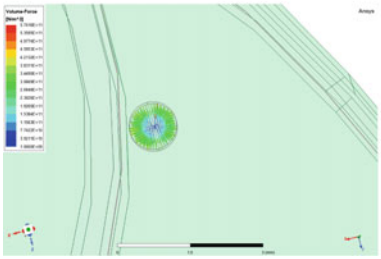

V2 with fully aligning contact assemble

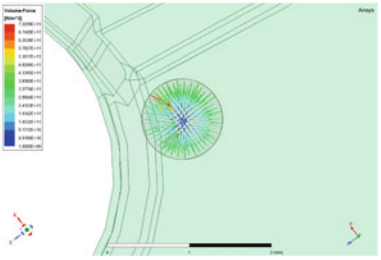

V2 with 15º dislocation assemble

Fig. 7 Volume force density of arc at 0.5 mm contact gap

Table 3 Electromagnetic force of arc at 0.5 mm contact gap (N)

Contact structure	F(x)	F(y)	F(z)	Mag(F)
V1 with contact area like V2	7.9	−1.4	0.9	8.1
V1 with contact area near central hole	−13.1	0.2	−0.2	13.1
V2 with fully aligning contact assemble	−4.3	0.2	3.8	5.7
V2 with 15° dislocation assemble	−6.2	−2.1	3.8	7.6

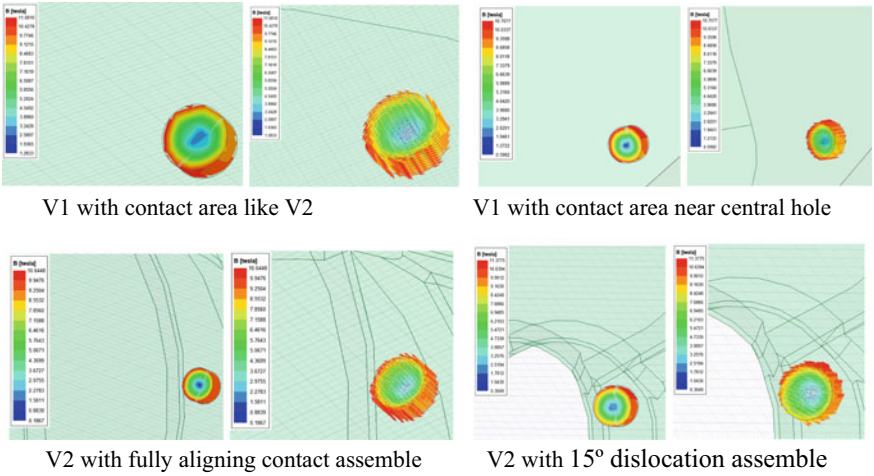

Fig. 8 Magnetic strength of arc at 0.5 mm contact gap

4 Conclusion

The electric repulsion of move contact can be decreased to 4% by improving contact structure at STC. It can improve the performance of short time withstand current (STC), peak withstand current and earthing switch making. The electromagnetic force direction of arc can be improved by improving contact structure. It can avoid arc erosion in a small area of contact and increase electric endurance performance. The electromagnetic force of arc can be increased by contact 15° dislocation assemble. It can increase the electric endurance performance of contact. The electric repulsion of move contact is about 190 N at 0.5 mm contact gap with arc for both contact structures. It can increase open speed at small contact gap. The maximum value of magnetic strength of arc is from 10.7 to 11.4 T at different situation, it is not much different. But the magnetic strength distribution is different.

References

1. Kojima H, Donen T, Kimura T, Kokura K, Hayakawa N (2020) Discrimination of discharge pattern in cut model of vacuum interrupter. In: XXIX international symposium on discharges and electrical insulation in vacuum, pp 323–326, Padova
2. Ge G, Cheng X, Liao M, Duan X, Zou J (2018) Vacuum arcs and postarc characteristic of vacuum interrupters with external AMF at current zero. IEEE Trans Plasma Sci 46(4):1003–1008
3. Falkingham LT (2017) The future of vacuum switchgear. In: 4th international conference on electric power equipment—switching technology. IEEE, China, pp 80–84
4. Li Y, Wang Z, Li Q, Geng Y, Wang J, Liu Z, Zhao X, Bi Y (2019) Vacuum arc characteristics of a novel contact consists of arcing contact and main contact. In: 5th international conference on electric power equipment—switching technology. IEEE, Japan, pp 174–178

5. Xiu S, Liu Z, Li R, Cui J, Liu T (2021) The influence of TMF and AMF components on arc movement characteristics in spiral-slot contacts. IEEE Trans Plasma Sci 49(4):1440–1447
6. Slade PG (2021) The vacuum interrupter: theory, design, and application, 2nd edn. CRC Press, Boca Raton
7. Li M, Wang X, Li W, Sun S (2015) Magnetic field and vacuum arc of new TMF-AMF contact. In: 3rd international conference on electric power equipment—switching technology (ICEPE-ST). IEEE, Korea, pp 270–273
8. Fan S, Yao X, Zhang J, Chen X, Liu Z, Wang J, Geng Y (2021) Fatigue failure of vacuum interrupter bellows in vacuum-type metal-enclosed gas-insulated switchgear. In: 2021 IEEE international conference on electrical engineering and mechatronics technology (ICEEMT 2021). IEEE, China, pp 254–257
9. Bhat R, Kulkarn SV (2018) Influence of contact plate parameters and eddy currents on residual flux decay in AMF-type vacuum interrupters. IEEE Trans Power Deliv 33(6):2812–2821

Partial Discharge Characteristics of Millimeter Metal Particle on a GIS Insulator Surface Under Long-Term Constant Voltage

Yiping Ji, Shaojing Wang, Xing Li, Guliang Zhou, Kai Gao, and Haoyang Tian

Abstract It is unavoidable for metal particle to be brought in gas-insulated switchgears (GISs) during the production, installation, and operation of the equipment. Currently, the metal particle is considered as one of the critical factors in insulation failures. In this paper, the partial discharge (PD) test of metal particle on the surface of an actual 220-kV insulator is performed under operation electric field of 1100 kV GIS insulators. Then the discharge characteristics of millimeter particle under a long-term constant voltage are investigated. The experiment result indicates that the PDs of metal particles is intermittent under working condition. In the initial period of the experiment, the discharge level can attain 9 pC, and a maximum of 150 discharges occur per second. Subsequently, when the test voltage keeps unchanged, the discharge level and repetition rate of PDs gradually decrease. Finally, the discharge tends to disappear within 60 min after the voltage application, and then suddenly become intense again briefly when $t = 210$ min and $t = 270$ min. The results in this paper gives an important basis for knowing the discharge characteristics of small metal particle well and can help to improve the reliability of GISs.

Keywords Gas-insulated switchgear (GIS) · Long-term constant voltage · Metal particle · Insulator surface · Partial discharge (PD)

Y. Ji · S. Wang · G. Zhou · K. Gao · H. Tian
Electric Power Research Institute of Shanghai Power Grid Corporation, Shanghai, China

X. Li (✉)
Sichuan Energy Internet Research Institute, Tsinghua University, Chengdu, Sichuan, China
e-mail: lx1230716@163.com

X. Dong and L. Cai (eds.), *The Proceedings of 2023 4th International Symposium on Insulation and Discharge Computation for Power Equipment (IDCOMPU2023)*, Lecture Notes in Electrical Engineering 1100, https://doi.org/10.1007/978-981-99-7393-4_2

1 Introduction

With the development of the power grid, ultra-high voltage (UHV) technique has become an important solution for large capacity and long-distance power transmission. Due to its excellent performance, the gas-insulated switchgears (GISs) are widely used in the power system [1, 2]. All the UHV substations in China have adopted GIS equipment. The reliability of the GIS equipment is crucial, which directly determines the security and stability of the grid. Considerable GIS insulation failures have occurred in field, causing huge economic losses and adverse social impact [3, 4].

During the manufacturing, installation and operation of a GIS, conductive particle may be brought into the equipment, greatly reducing the insulation performance of GIS [5]. At present, the metal particle is still regarded as a critical factor in insulation failures [6]. Hence, it is urgent to investigate the surface discharge characteristics of particles on the insulation surface in a GIS.

Extensive research has been carried out to investigate the insulator surface insulation performance with metal particles in the GIS [7, 8]. However, in previous studies, particles longer than 1 cm are usually used to study the PD characteristics [9, 10], and the research on shorter particles (<1 cm) are mainly performed on a scaled model [11, 12]. Obviously, these are inconsistent with the actual conditions in an actual GIS. The metal particles in an actual GIS equipment are usually millimeter or even micrometer in length [13], and the GIS insulator, especially the ultra-high voltage GIS insulator, is much larger than the metal particles. The previous research focusing on the centimeter particle and scaled models seems to have limited guidance on engineering applications, and the results cannot explain the fault phenomenon in field well.

An experimental platform for PD test is established in this study, which can be employed for long-term continuous PD test for GIS insulators. Then, the PD test for 4-mm long metal particles on a GIS insulation surface is performed under operation electric field of the UHV GIS insulator. The discharge characteristics under a long-term constant voltage are obtained, and the PRPS patterns at different times are investigated. The results of this paper give an important basis for knowing the discharge characteristics of metal particle and is also helpful for improving the reliability of the GIS.

2 Experiment Arrangement

2.1 Experiment Platform

In this paper, an experiment platform is established for long-term PD test, which can realize the PD measurement of multiple insulators. The platform mainly includes an armored test transformer, three test units and a PD detection system as shown

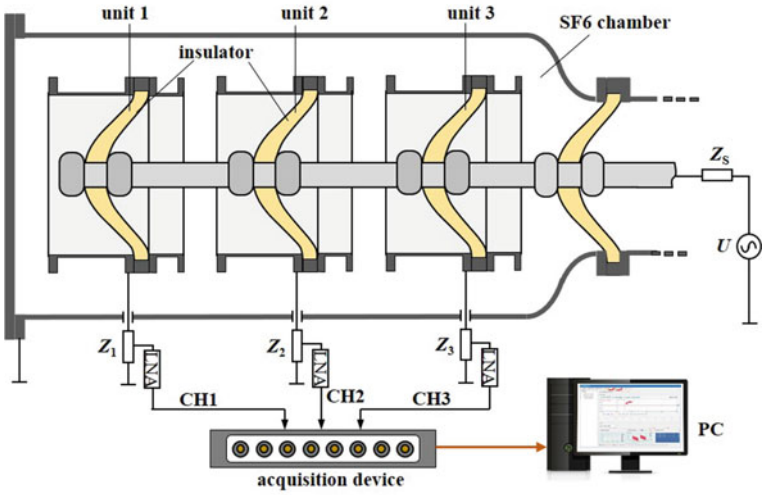

Fig. 1 Experimental platform

in Fig. 1. Each test unit is composed of a 220-kV insulator. The enclosures of the three units are insulated from each other and three detection impedances Z_1–Z_3 are connected to the enclosure of the three units respectively. The center electrode of the three test GIS insulators is connected to the power supply (U) via the protection resistance (Z_S). During the test, the test units are placed in the chamber filled with SF_6 gas (0.4 MPa).

2.2 PD Detection System

The PD detection system shown in Fig. 1 consists of three detection impedances Z_1–Z_3, which are used to measure PDs of the three test insulators respectively. A low-noise amplifier (LNA, bandwidth: 100–500 kHz, gain: 50 dB) is applied to pre-amplify the PD signals. The analog bandwidth and maximum sampling rate of the data acquisition device are 200 MHz and 1 GS/s respectively.

According to the method proposed in our previous study [14], the interference and discharge pulse can be identified reliably. The channels 1–3 represent the outputs of detection impedance Z_1–Z_3, respectively. As shown in Fig. 2a, when obvious pulse appears in the channel CH1, and the pulse appearing in channels CH2 and CH3 is very small. In this case, the pulse can be considered to be generated by discharge in unit 1. Similarly, as displayed in Fig. 2b and c, when the amplitude detected by Z_2 and Z_3 is far greater than that of others, the signals can be determined as discharges generated by the insulator in test unit 2 and 3 respectively. As indicated in Fig. 2d, the

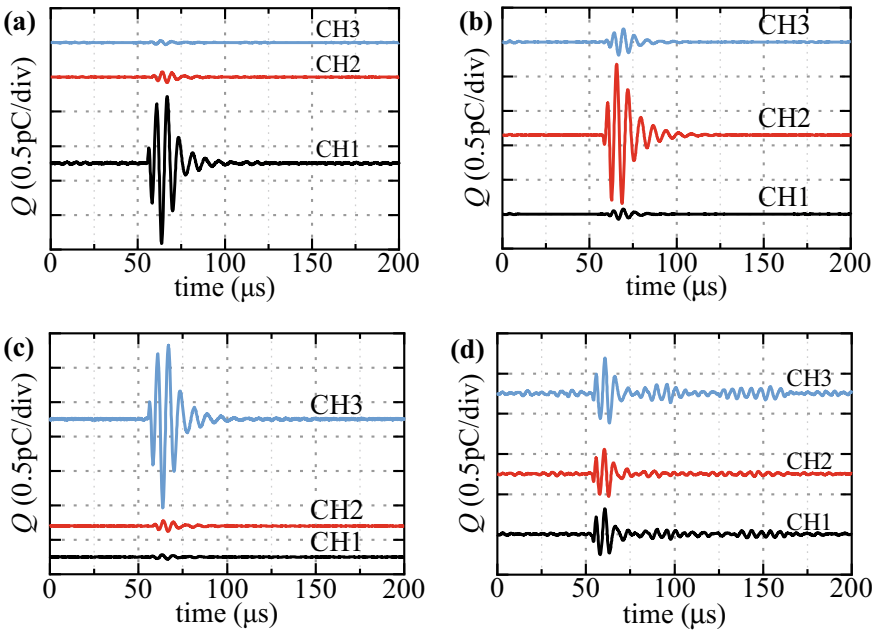

Fig. 2 PD and interference pulse identification: **a** PD occurs in unit 1, **b** PD occurs in unit 2, **c** PD occurs in unit 3, **d** external interference occurs

signal amplitude of CH1–CH3 is close to each other, so the signals can be considered to be caused by interference.

The calibration result based on IEC method [15] indicates that the detection sensitivity of the PD system is 0.2 pC.

2.3 Experimental Model

In order to obtain the real operation condition of a 1100 kV GIS insulator, factors such as electric field intensity and distribution, and surface insulation distance should be considered when selecting the experimental model. Firstly, the surface insulation distance of the test insulator should be far greater than particle length. Secondly, the electric field (including the intensity and distribution) on the test insulator surface should be closed to that on the UHV insulator surface under working conditions ($U_{\mathrm{rms}} = 635$ kV for 1100 kV insulators).

For above considerations, an actual 220-kV insulator is selected as the experimental model in this paper. The surface insulation distance of the 220-kV insulator is approximately 170 mm, which is dozens of times the metal particle length. Moreover, as illustrated in Fig. 3, when the test voltage of 270 kV (effective value) is

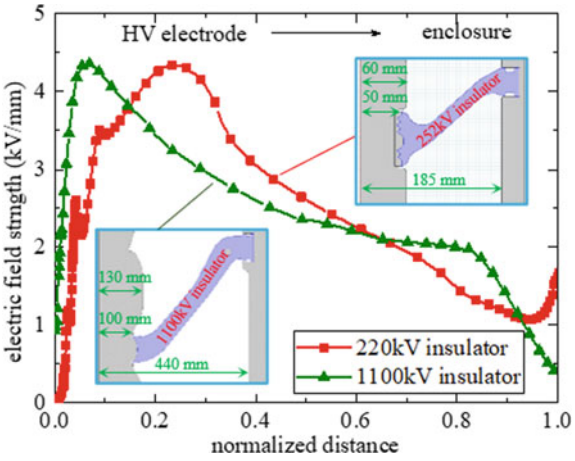

Fig. 3 Electric field on the actual 220-kV and 1100-kV GIS insulator surface

applied, the electric field on the test insulator surface is closed to that on a UHV insulator surface under working conditions.

2.4 Defect Setting

In our previous research, it has been found that the critical length of metal particles that cause surface flashover of 1100 kV insulators under operating conditions is approximately 5 mm [16]. Consequently, in this study, cylindrical aluminum metal particles with a diameter of 0.5 mm and a length of 4 mm are selected as defect to investigate long-term discharge characteristics. As shown in Fig. 4, the defect is set at the position where the electric field intensity is the largest on the concave surface (4.5 cm away from the high-voltage electrode).

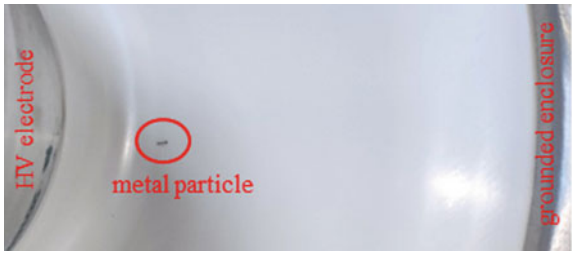

Fig. 4 Defect setting

2.5 *Voltage Application*

To obtain the operation condition of a 1100 kV GIS insulator, the test voltage of 270 kV should be applied to a 220-kV insulator. Hence, during the test, the voltage is applied as: 127 kV for 3 min, then 175 kV and 200 kV for 5 min, and 270 kV for 6 h.

3 Experiment Results

3.1 *PD Characteristics*

When no defects are set, the test voltage of 270 kV is applied for 10 min. The discharge level under this voltage is lower than 0.2 pC (lower than the detection sensitivity).

Then the metal particle is set on the concave surface of all three insulators, and the voltage is applied according to the above-mentioned method. The PD measurement is performed continuously during the experiment. It is found that the PD characteristics of the three insulators are similar. Here is an example of the insulator in test unit 3.

Figure 5 shows the PD characteristics under step voltage. It can be seen that there is no discharge under only 127 kV. Then, the PD occurs under 175 kV. However, the discharges are weak and intermittent. The discharge level is lower than 1 pC, and only approximately 10 discharges appear within a second. Under 200 kV, the discharge level and discharge number increase slightly. Under 270 kV, the discharge level and repetition rate of PDs both increase significantly. The discharge level can exceed 5 pC, and a maximum of 150 discharges occur per second.

Figure 6 shows the PD characteristics under long-term constant voltage. It can be seen that under the voltage of 270 kV, the PDs are intense in the initial period. Subsequently, the discharge level and discharge repetition rate both begin to decrease. The

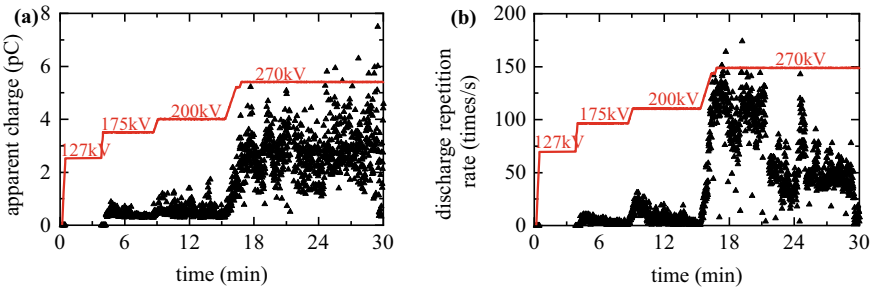

Fig. 5 PD characteristics under step voltage: **a** maximum discharge level per second, **b** discharge number per second

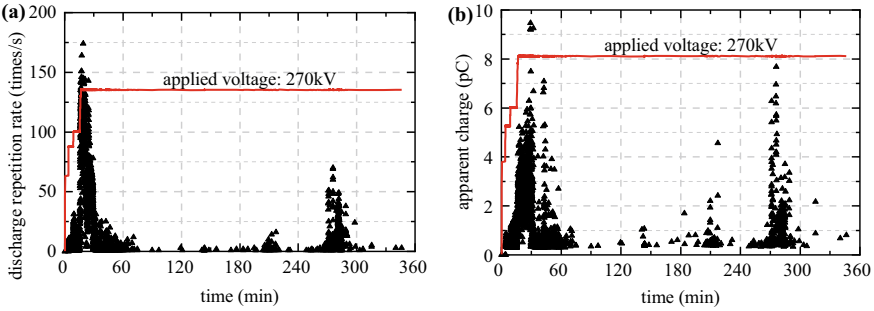

Fig. 6 PD characteristics under long-term constant voltage: **a** discharge number per second, **b** maximum discharge level per second

discharges became weak and intermittent. Approximately 60 min after the voltage is increased to 270 kV, the discharge tends to disappear. Then when $t = 210$ min and $t = 270$ min, the PD becomes intense again temporarily. Especially when $t = 270$ min, more than 70 discharges occur in one second at most, and the maximum discharge level can attain approximately 8 pC.

Figure 7 shows the PRPS patterns at different moments during the test. When the voltage is low, discharges only occur in the negative half cycle, as displayed in Fig. 7a. With the increase of the test voltage, the discharges begin to appear in the positive half cycle. However, the discharge level (Q) is still very low, as illustrated in Fig. 7b and c. When the voltage is maintained at 270 kV, the discharge becomes intense, and the discharges in the negative half cycle is significantly stronger than that in the positive half cycle, as displayed in Fig. 7d. Then under constant voltage, the PDs gradually weakens. After about 30 min, the discharge becomes sporadic, as shown in Fig. 7e and f. When $t = 270$ min, the discharges become severe again, and the discharge in the negative half cycle is stronger than that in the positive half cycle, as shown in Fig. 7h.

The above results show that under long-term constant voltage, the discharge of meal particle on a GIS insulator surface is intermittent, which is consistent with some fault phenomenon in the field. Although the discharge is relatively weak and sporadic, with the development of surface discharge and surface charge accumulation, the insulator flashover will eventually occur [16]. Therefore, in field detection, the sensitivity and anti-interference ability of PD detection method need to be further improved to capture the weak and intermittent discharge pulses. Meanwhile, in online detection and monitoring, those weak and intermittent signals, as well as the signals that disappear and then appear again briefly, need to be given more attention. Moreover, it is also a feasible method to comprehensively monitor and analyses the PD signals in a longer period, which can help to avoid the misjudgment caused by the intermittent discharge.

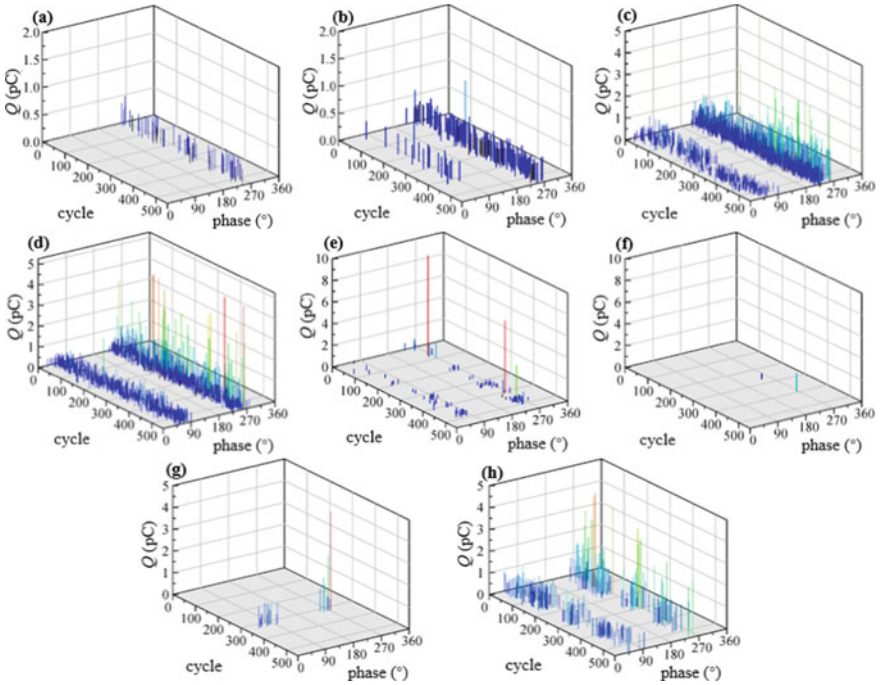

Fig. 7 PRPS patterns of the particles during the test: **a** $t = 5$ min 10 s–5 min 20 s, **b** $t = 10$ min 50 s–11 min 0 s, **c** $t = 16$ min 30 s–16 min 40 s, **d** $t = 20$ min 50 s–21 min 0 s, **e** $t = 31$ min 50 s–32 min 0 s, **f** $t = 60$ min 0 s–60 min 10 s, **g** $t = 231$ min 30 s–231 min 40 s, **h** $t = 270$ min 0 s–270 min 10 s

4 Conclusion

In this study, the PD test of 4-mm long particle on an actual 220-kV basin insulator surface under long-term constant voltage is conducted, and the discharge characteristics are obtained.

(1) The PD increases with the increase of test voltage. When the test voltage is lower than 200 kV, the discharge level is smaller than 2 pC, and there are less than 30 discharges in one second. Under 270 kV (the operation condition of a UHV GIS insulator), the discharge is enhanced markedly, and the discharge level can exceed 9 pC.

(2) Under working condition, the discharge is intermittent. When the voltage is kept at 270 kV, the discharge level and repetition rate of PDs firstly increase and then gradually decrease within 60 min. Then, under long-term constant voltage, the PD rends to disappear and suddenly become intense again in a period.

(3) It is necessary to promote the sensitivity and anti-interference performance of PD detection method to capture and identify the weak and intermittent PDs. Through PD detection and diagnosis during a longer period, the misjudgment and missed judgment can be avoided.

Acknowledgements The authors gratefully acknowledge the support of the Scientific and Technological Project of State Grid Corporation of China (program 52094022004A).

References

1. Okubo H, Beroual A (2011) Recent trend and future perspectives in electrical insulation techniques in relation to sulfur hexafluoride (SF_6) substitutes for high voltage electric power equipment. IEEE Electr Insul Mag 27(2):34–42
2. Riechert U, Holaus W (2011) Ultra high-voltage gas-insulated switchgear—a technology milestone. Eur Trans Electr Power 22(1):60–82
3. Dreisbusch K, Kranz H, Schnettler A (2008) Determination of a failure probability prognosis based on PD—diagnostics in GIS. IEEE Trans Dielectric Electr Insul 15(6):1707–1714
4. Schichler U, Koltunowicz W, Endo F et al (2013) Risk assessment on defects in GIS based on PD diagnostics. IEEE Trans Dielectric Electr Insul 20(6):2165–2172
5. Wang H, Xue JY, Chen JH et al (2019) Effects of metal particle material on surface flashover performance of alumina-filled epoxy resin spacers in SF_6/N_2 mixtures under DC voltage. AIP Adv 9(8):085212
6. Okabe S, Yamagiwa T, Okubo H (2008) Detection of harmful metallic particles inside gas insulated switchgear using UHF sensor. IEEE Trans Dielectric Electr Insul 15(3):701–709
7. Wang J, Hu Q, Chang YN et al (2021) Metal particle contamination in gas-insulated switchgears/gas-insulated transmission lines. CSEE J Power Energy Syst 7(5):1011–1025
8. Liang RX, Hu Q, Liu H et al (2022) Research on discharge phenomenon caused by cross-adsorption of linear insulating fibre and metal dust under DC voltage. High Voltage 7(2):269–278
9. Zhao CH, Tang ZG, Zhang LG et al (2020) Entire process of surface discharge of GIS disc-spacers under constant AC voltage. High Voltage 5(5):591–597
10. Qi B, Li CR, Hao Z et al (2011) Surface discharge initiated by immobilized metallic particles attached to gas insulated substation insulators: process and features. IEEE Trans Dielectric Electr Insul 18(3):792–800
11. Wu ZC, Lyu B, Zhang QG et al (2020) Phase-space joint resolved PD characteristics of defects on insulator surface in GIS. IEEE Trans Dielectric Electr Insul 27(1):156–163
12. Budiman FN, Khan Y, Malik NH et al (2013) Utilization of artificial neural network for the estimation of size and position of metallic particle adhering to spacer in GIS. IEEE Trans Dielectric Electr Insul 20(6):2143–2151
13. You H, Zhang QG, Guo C et al (2017) Motion and discharge characteristics of metal particles existing in GIS under DC voltage. IEEE Trans Dielectric Electr Insul 24(2):876–885
14. Li X, Liu WD, Xu Y et al (2022) Discharge characteristics and detectability of metal particles on the spacer surface in gas-insulated switchgears. IEEE Trans Power Delivery 37(1):187–196
15. High-voltage test techniques—partial discharge measurements, 60270, Standard of International Electro-technical Commission (IEC) (2001)
16. Li X, Liu WD, Xu Y et al (2020) Surface charge accumulation and pre-flashover characteristics induced by metal particles on the insulator surfaces of 1100 kV GILs under AC voltage. High Voltage 5(2):134–142

Ultrasound-Based Pressure Pipe Internal Water Ingress Defect Detection Technology

Wenhui Li, Haibo Li, Yian Fang, Huan Liu, Junzhe Liang, Fenggeng Jiang, Guang Liu, and Di Rao

Abstract Long-term operation in the harsh environment of the tension clamp aluminum tube unpressed area, easy to produce water ingress defects. Based on the reflection characteristics of ultrasound, the optimal detection position, the best detection frequency and the echo characteristics of the internal water inlet in the unpressurized area were studied, and a method for ultrasonic detection of the internal water ingress of the tension-resistant clamp was proposed. The results show that observing the reception time of the primary echo at the water–air interface can determine whether water ingress occurs in the unpressurized area and what the inlet depth is. This method provides a new idea for detecting water ingress inside the tension clamp.

Keywords Transmission lines · Tension clamp · Ultrasonic · Water ingress defects

1 Introduction

Tension clamp is one of the important fittings of transmission lines, which is used to fix the conductor or lightning protection wire on the tensile insulator string of the non-linear pole tower to play the role of anchoring and conduction [1, 2]. At present, the use of tensile clamps and connecting pipe crimping is the only means to realize long-distance uninterrupted transmission of ultra-high voltage transmission lines [3]. With the rapid development of the power grid, the voltage level is getting higher and higher, and the performance defects of tensile clamps have become an important factor

W. Li · Y. Fang · H. Liu · J. Liang · G. Liu
State Grid Zhejiang Electric Power Co., Ltd., Taizhou Power Supply Company, Zhejiang 318000, China

H. Li · D. Rao (✉)
Taizhou Hongchuang Power Group Co., Ltd., Technology Branch17, Zhejiang 318000, China
e-mail: 978516547@qq.com

F. Jiang
State Grid Zhejiang Xinxing Technology Co., Ltd, Zhejiang 318000, China

X. Dong and L. Cai (eds.), *The Proceedings of 2023 4th International Symposium on Insulation and Discharge Computation for Power Equipment (IDCOMPU2023)*, Lecture Notes in Electrical Engineering 1100, https://doi.org/10.1007/978-981-99-7393-4_3